

Kinetic and structural analysis of mutant CD4 receptors that are defective in HIV gp120 binding

HAO WU*[‡], DAVID G. MYSZKA^{‡§¶}, SUSAN W. TENDIAN^{||}, CHRISTIE G. BROUILLETTE^{||}, RAY W. SWEET[§], IRWIN M. CHAIKEN^{§**}, AND WAYNE A. HENDRICKSON*[†]

*Department of Biochemistry and Molecular Biophysics and [†]Howard Hughes Medical Institute, Columbia University, New York, NY 10032; [§]SmithKline Beecham Pharmaceuticals, King of Prussia, PA 19406; and ^{||}Southern Research Institute, Birmingham, AL 35205

Contributed by Wayne A. Hendrickson, October 18, 1996

ABSTRACT The T-cell antigen coreceptor CD4 also serves as the receptor for the envelope glycoprotein gp120 of HIV. Extensive mutational analysis of CD4 has implicated residues from a portion of the extracellular amino-terminal domain (D1) in gp120 binding. However, none of these proteins has been fully characterized biophysically, and thus the precise effects on molecular structure and binding interactions are unknown. In the present study, we produced soluble versions of three mutant CD4 molecules (F43V, G47S, and A55F) and characterized their structural properties, thermostability, and ability to bind gp120. Crystallographic and thermodynamic analysis showed minimal structural alterations in the F43V and G47S mutant proteins, which have solvent-exposed mutant side chains. In contrast, some degree of disorder appears to exist in the folded state of A55F, as a result of mutating a buried side chain. Real time kinetic measurements of the interaction of the mutant proteins with gp120 showed affinity decreases of 5-fold for G47S, 50-fold for A55F, and 200-fold for F43V. Although both rate constants for the binding reaction were affected by these mutations, the loss in affinity was mainly due to a decrease in on rates, with less drastic changes occurring in the off rates. These observations suggest the involvement of conformational adaptation in the CD4–gp120 interaction. Together, the structural and kinetic data confirm that F43V is a critical residue in gp120 recognition site, which may also include main chain interactions at residue Gly-47.

The cell surface glycoprotein CD4, expressed predominantly on T-helper cells, plays important roles in both thymic development of T cells and their antigen-dependent activation in the periphery (1). CD4 participates in the antigen recognition complex through its extracellular association with major histocompatibility complex class II on antigen-presenting cells and close association with the T-cell receptor itself (2–4) and through intracellular signaling mediated by its association with the src-like lymphocyte tyrosine kinase p56^{lck} (5, 6). HIV subverts human CD4 to serve as its receptor for cellular attachment (7–9). The binding of the viral external envelope glycoprotein gp120 to CD4 appears to trigger rearrangement of the envelope complex (ref. 10 and references therein), leading to fusion of viral and cellular membranes and the delivery of the viral core into host cells. This same interaction is thought to initiate envelope-mediated fusion between infected and uninfected CD4 cells (11, 12). Recent studies revealed that the hallmark slow progressive loss of CD4⁺ cells in HIV-infected individuals belies a dynamic raging viral infection in contest with immune-mediated elimination of infected cells and cell renewal (13, 14). Thus, blockade of the initial interaction of CD4 with gp120 has potential as a therapeutic target for the treatment of HIV infection and AIDS.

The extracellular region of CD4 consists of four tandemly arranged and intron-separated immunoglobulin-like domains, as first suggested by sequence comparisons and later confirmed by the crystallographic studies of the membrane distal two-domain fragment (D1D2) of human CD4 (15–17) and the membrane proximal two-domain fragment (D3D4) of rat CD4 (18). The binding site for gp120 resides within the amino-terminal domain, D1 (9, 19, 20). This domain is homologous to the variable domain of antibodies with the characteristic topology of two β sheets of four and five strands. Compared with immunoglobulins, the CDR2-like region in D1 (C'–C'') is extended. Extensive mutational analysis centers the gp120 binding site in this region of D1 (17). The mutational data, when screened against indirect effects by solvent accessibility criteria based on the native D1D2 structure, implicated the side chains of residues Lys-35, Phe-43, and Arg-59 in direct interaction with gp120, with possible contributions from Leu-44 and Lys-46 (17). The conservation of this binding site is shown by the similar, although not identical, recognition of CD4 by recombinant gp120 proteins from diverse isolates (ref. 20 and unpublished results). However, precise interpretation of the mutational results is hampered by the uncertain effects of sequence changes on molecular structure and binding dynamics.

In this report, we examined three mutants of CD4 using a combination of kinetic, structural, and thermodynamic approaches. The three mutations, F43V, G47S, and A55F, were chosen for their differing effect on recognition of gp120. Each was created in the construction of D1D2, which contains the first two domains of CD4 and the entire gp120 binding region. Residue Phe-43, whose side chain protrudes into the solvent, lies at the center of the cluster of residues implicated in binding. While some conservative substitutions have little effect on binding, other substitutions, including valine (19), at this position showed a markedly reduced affinity (refs. 19–22; unpublished results). Like F43V, the A55F mutation was previously shown to severely reduce binding to gp120 (19). Because this residue is buried in the hydrophobic core underpinning CDR2, the mutation was presumed to perturb the binding site indirectly (17). Consistent with this interpretation, mutation of Ala-55 to other hydrophobic residues such as valine, isoleucine, and leucine have only a 2- to 3-fold effect on binding (ref. 20 and unpublished results). Gly-47 lies at the distal end of the C' strand and the serine substitution modestly reduced binding in ELISA-based interaction assays (unpublished results). Through analysis of these mutants, we sought

Data deposition: The atomic coordinates have been deposited in the Protein Data Bank, Chemistry Department, Brookhaven National Laboratory, Upton, NY 11973 [references 1cdj (native), 1cdu (F43V), and 1cdy (G47S)].

[‡]H.W. and D.G.M. contributed equally to this work.

[¶]Present address: Department of Oncological Sciences, Huntsman Cancer Institute, University of Utah, Salt Lake City, UT 84132.

^{**}Present address: University of Pennsylvania, School of Medicine, 913 Stellar Chance Labs, 422 Curie Boulevard, Philadelphia, PA 19104.

The publication costs of this article were defrayed in part by page charge payment. This article must therefore be hereby marked "advertisement" in accordance with 18 U.S.C. §1734 solely to indicate this fact.

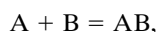
to define the role of Phe-43 in recognition of gp120 and to deduce other potential contributions by main or side chain residues. Our structural and thermodynamic analysis reveals minimal structural alteration in the F43V and G47S molecules outside of the side chains themselves, whereas A55F was found to be structurally perturbed and also failed to yield crystals. Our real-time kinetic binding data from BIAcore (Pharmacia Biosensor) measurements showed that the decrease in affinity for gp120 binding by these mutated CD4 molecules is mainly due to a decrease in association rates. This effect may suggest involvement of conformational adaptation in CD4–gp120 interaction.

MATERIALS AND METHODS

Protein Preparation. The production and isolation of the recombinant human sCD4 and D1D2 proteins and the creation of the sCD4 mutants F43V and A55F have been described (15, 19, 23, 24). The G47S variant was created by oligonucleotide-directed mutagenesis in sCD4 containing pAlter-1 (Promega)-based plasmid. Each mutation was cloned into a D1D2 expression plasmid and produced in CHO cells in a manner similar to that described for D1D2 itself (15), except that these proteins terminate at residue 183 without the two carboxyl-terminal missense amino acids, Asn-Thr. The F43V and A55F proteins were purified by ion exchange and size exclusion chromatography (15, 24). Due to its lower production level, the G47S protein was purified by immunoaffinity chromatography with the CD4 mAb L71 (Becton Dickinson). The recombinant gp120 (HIV-1/BH-10) has been described (25). All proteins were assessed to be >90% pure by reducing SDS/PAGE.

Kinetic Measurement and Analysis. The kinetics of gp120 binding to sCD4, D1D2, and the mutant proteins F43V, G47S, and A55F were determined by the technique of surface plasmon resonance with a BIAcore instrument (Pharmacia Biosensor). Each form of CD4 was coupled to a separate CM5-certified sensor chip surface using standard amine coupling procedures described previously (26, 27). Immobilization levels were kept as low as possible to minimize mass transport effects and steric hindrance. Typically, the immobilization levels were around 500 response units (RU) for sCD4 and 250 RU for the different D1D2s. Binding experiments were performed at 25°C in buffer of pH 7.4 containing 150 mM sodium chloride, 10 mM Hepes, 3.4 mM EDTA disodium salt, and 0.005% Tween 20. Association was measured by passing various concentrations of gp120 over the different CD4 surfaces in 25- μ l injections at a flow rate of 5 μ l/min. Response plateaus were at a level indicating that only roughly one-fourth of the CD4 was active on the surface, but this effect was the same for all forms of CD4. After the injection, dissociation of bound gp120 was monitored by washing the surface with buffer for 300 sec. The remaining gp120 was removed and a fully active chip surface was regenerated with a 3- μ l injection of 100 mM phosphoric acid at a flow rate of 25 μ l/min. The interaction of gp120 with sCD4, D1D2, and G47S was measured over a concentration range of 50–750 nM. The binding to A55F and F43V was monitored at gp120 concentrations ranging from 0.75 to 6 μ M and 1 to 10 μ M, respectively. These kinetic binding studies were repeated three times for each form of CD4 (except for G47S), starting with a new sensor surface for each experiment. For some experiments, the assay was reversed to measure CD4 binding to immobilized gp120.

Binding kinetics were evaluated with relationships described previously (28) for a simple bimolecular interaction:



where

$$dR/dt = k_{\text{on}}[A]R_{\text{max}} - (k_{\text{on}}[A] + k_{\text{off}})R. \quad [1]$$

Here k_{on} and k_{off} are the on- (association) and off- (dissociation) rate constants, respectively. $[A]$ is the concentration of analyte in solution and B is the immobilized ligand. R is the relative response unit of the biosensor at time t , which is proportional to the complex formed. R_{max} is the maximum response. Under these assumptions, a plot of dR/dt versus R should give a straight line with a slope of $k_s = -(k_{\text{on}}[A] + k_{\text{off}})$. A replot of k_s versus $[A]$ will yield a slope k_{on} . During the elution phase, $[A]$ is assumed to be zero, and therefore:

$$dR/dt = -k_{\text{off}}R. \quad [2]$$

A plot of $\ln(R_0/R)$ versus t from the dissociation phase should have a straight line with a slope of k_{off} . Alternative methods of analysis, including fits with two exponentials, were tried but not pursued because of model dependence. Instead, only the early phase kinetics were used to compare behavior of the various CD4 molecules.

Stability Measurements. Thermodynamic measurements of urea-induced unfolding were performed as described earlier for CD4 and D1D2 (29) and were used to determine the stability of mutants F43V and A55F as compared with native D1D2. The absorption and fluorescence emission unfolding data were fit concurrently by a global analysis to a two-state unfolding model, whereby the unfolding free energy in water and its urea dependence were derived.

Crystallization. All protein samples were crystallized by the hanging drop vapor diffusion method (30). The drops contained 3 μ l of 10–30 mg of protein per ml of PBS buffer plus 3 μ l of reservoir solution. For native D1D2 and F43V, the reservoirs contained 23% (15) and 25% PEG 3350, respectively. For G47S, the reservoirs were 28% PEG 3350 in 50 mM Hepes buffer at pH 8.2. All three forms of crystals were stabilized in 100 mM Tris (pH 8.5) and 30% PEG 3350, with 20% glycerol added for data collection at 110 K. A55F has failed to crystallize in various crystallization attempts including the factorial search, grid search with various precipitants and different pH, and combinations of salt and PEG.

Diffraction Measurement and Structure Refinement. Diffraction data for native D1D2 crystal were collected at 110 K on an R -axis area detector system and images were processed with DENZO/SCALEPACK (31). Data of F43V were measured at room temperature on a Xuong–Hamlin multiwire area detector, integrated with program XDS (ref. 32; D. Diggs & K. Watkins, personal communication) and scaled with the CCP4 package (33). Diffraction measurements for G47S were done at 110 K at the Howard Hughes Medical Institute X4A beam line of the National Synchrotron Light Source (NSLS) at Brookhaven National Laboratory on Fuji imaging plates. These data were processed with DENZO (31) and scaled with the CCP4 package (33).

The type I native D1D2 structure (Protein Data Bank reference 1cdh; protein atoms only) was directly placed into the new crystal cells and refined as a rigid body. This was then followed by stereochemically restrained simulated annealing refinement (34). The $2|F_o| - |F_c|$ maps at this point provided clear guidance for the building (35) of mutated side chains. After further refinement and addition of solvent molecules, simulated annealing omit maps were used to confirm the mutations.

RESULTS

Kinetic Analysis of gp120–CD4 Interaction. The surface plasmon resonance sensograms for gp120 binding to immobilized sCD4, D1D2, A55F, and F43V are shown in Fig. 1 (similar experiments performed for G47S are not shown). The response curves for sCD4 and D1D2 are very similar, but higher concentrations of gp120 are required to achieve binding to A55F and F43V, indicating a weaker affinity for these

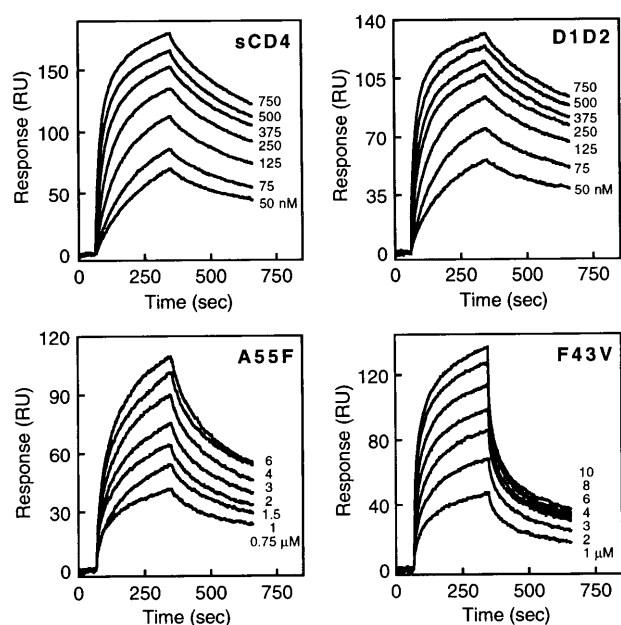


FIG. 1. Sensorgram overlays for gp120 binding to sCD4, D1D2, A55F, and F43V surfaces. Binding responses were zeroed before injection, and the refractive index change was subtracted out of the association phase by passing the sample over a blank surface. The concentration of gp120 injected over the surface is shown at the right of each sensorgram.

mutants. Fig. 2 shows a linear transformation of the association phase for sCD4 and of the dissociation phases overlaid for all forms of CD4. A one-step bimolecular interaction model fits the binding data at the early portions of the association and dissociation phase, but nonlinearity becomes apparent at the later time points for each form of CD4. Similar kinetics were also observed for sCD4 binding to immobilized gp120. In general, a number of instrument artifacts or complex protein interactions have been invoked to explain the nonlinear behavior often observed in biosensor data (36, 37). Increasing the flow rate or adding soluble CD4 to the dissociation phase buffer did not alter the shapes of the gp120 binding responses, indicating that mass transport was not the cause of the deviations (37). By analytical ultracentrifugation at comparable concentrations, gp120 and CD4 alone were shown to behave as monomers and form a 1:1 complex when mixed (P. Hensley, personal communication), which suggests that self-association was not the root of the deviations. We cannot rule out surface heterogeneity imposed by the random amine coupling procedure. Finally, this complexity may arise from a genuine multistep binding reaction. Since all of the CD4 proteins showed the same nonlinear behavior with respect to gp120 binding, to directly compared the effects of the mutations, we analyzed the early portions of the association and

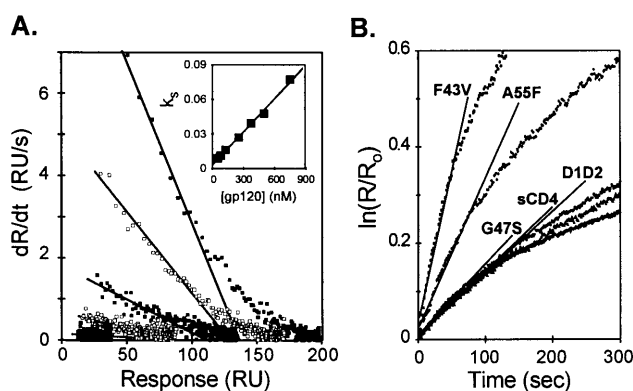


FIG. 2. Kinetic analysis. (A) A linear transformation of the association phase data for gp120 binding to a sCD4 surface. The straight lines are a linear least squares fit to the response data (\square and \blacksquare) acquired at the selected gp120 concentrations of 750, 375, 125, and 50 nM. The k_s values determined from these slopes were replotted versus gp120 concentration shown in the *Inset* (\circ), providing the on rate constant. (B) A linear transformation of the dissociation phase data for the highest concentration of gp120 injected over each form of CD4 surface. The slope of the straight line, labeled for each CD4 surface, was fit to the initial 90 sec of the transformed dissociation phase data and provided the off-rate constant.

dissociation phases, which constituted the majority of the binding response.

Table 1 shows the apparent association and dissociation constants derived from linearization analysis of the biosensor data and the corresponding calculated equilibrium dissociation constants. The standard deviations reported for each parameter were experimentally determined by repeating each biosensor experiment three times starting with the immobilization. The rate constants for gp120 binding to sCD4 and D1D2 were found to be nearly identical, indicating that domains 3 and 4 do not contribute to the binding reaction and that the association reaction is not diffusion controlled. The mutant proteins showed changes in both the on- and off-rate constants, leading to an overall decrease in affinity of 5-fold for G47S, 50-fold for A55F, and 200-fold for F43V. But as shown in Table 1, the on-rate constants were reduced more drastically, by 3- to 50-fold, whereas the off-rates were increased by only 1.5- to 4-fold.

Stability of Native and Mutant D1D2. Urea-induced denaturation of the mutants A55F and F43V was measured and compared with the unfolding of native D1D2, which has been previously presented (29). The unfolding curves measured by absorbance and fluorescence were fit concurrently to a two-state unfolding model and are shown along with the fits in Fig. 3. The thermodynamic parameters obtained from curve fitting are given in Table 1. As shown earlier for native D1D2 unfolding, the absorption and emission data for both A55F and F43V fit fairly well to the equation derived from a two-state unfolding model. Fig. 3 shows that the urea-dependent unfolding profile of A55F is unlike that of native D1D2 and F43V.

Table 1. Summary of kinetic and stability data

CD4 molecule	k_{on} , $M^{-1}\cdot s^{-1}$ $\times 10^{-3}$	k_{off} $s^{-1} \times 10^3$	K_d^* , $M \times 10^8$	$\Delta G_{H_2O}^\dagger$ kcal/mol	$m,^\ddagger$ kcal/(mol·M)	[Urea] $_{1/2}$, M
sCD4	83 ± 12	1.6 ± 0.4	1.9 ± 0.5	3.74 ± 0.96	2.26 ± 0.64	3.11
D1D2	82 ± 22	1.5 ± 0.3	1.8 ± 0.6	2.5 ± 0.2	1.09 ± 0.08	2.3
F43V	1.7 ± 0.4	6.2 ± 3.0	360 ± 200	2.9 ± 0.4	1.13 ± 0.16	2.5
G47S	$26 \pm ND$	$2.3 \pm ND$	$9.0 \pm ND$	ND	ND	ND
A55F	3.3 ± 0.7	2.9 ± 0.8	90 ± 30	2.6 ± 0.2	0.75 ± 0.08	3.5

ND, not determined.

* K_d is calculated from k_{off}/k_{on} .

‡ The thermodynamic parameters, ΔG_{H_2O} and m , obtained from curve fitting, are shown as 95% confidence intervals, assuming a normal distribution of the errors.

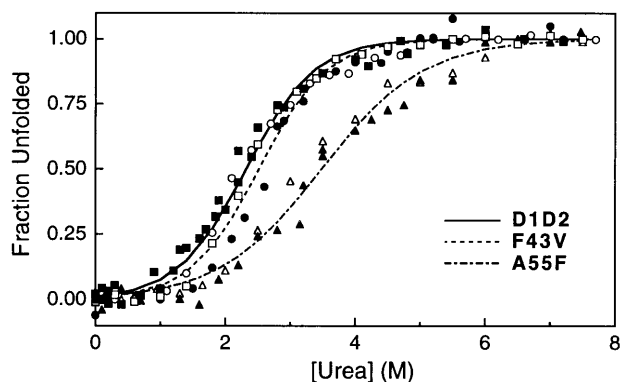


FIG. 3. Urea unfolding of D1D2 (\square and \blacksquare), F43V (\circ and \bullet), and A55F (\triangle and \blacktriangle). For each protein, the urea concentration dependence of the fractional changes in delta absorbance (open symbols) and delta fluorescence (solid symbols) were fit concurrently to a two-state unfolding model. These fits are shown as a solid line for D1D2, a dotted line for F43V, and a dashed line for A55F.

Comparison of the thermodynamic parameters indicates that this difference arises from a difference in the urea dependence of the unfolding free energy, m , and not from a difference in ΔG_{H_2O} , as native D1D2 and A55F are approximately equal in stability in water. The m values for native D1D2 and F43V are essentially identical while the m value for A55F is significantly smaller. A smaller m is expected to indicate either less structure in the folded state or greater residual structure in the unfolded state compared with the wild type (38). A55F is buried in the structure and the difficulty in obtaining crystals of A55F support the hypothesis that some degree of disorder exists in the folded state of A55F. This destabilizing effect and the enhanced hydrophobic effect from burying the larger hydrophobic residue seem to cancel each other and result in the observed near-equivalency of ΔG_{H_2O} for A55F and native D1D2. F43V is slightly more stable in water than D1D2 or A55F, probably as a result of a relieved reverse hydrophobic effect resulting from substitution of a less hydrophobic valine for the highly exposed phenylalanine [fractional solvent accessibility = 0.8 (15)]. The reverse hydrophobic effect has been described as the destabilizing effect caused by hydrophobic residues when they are more exposed to solvent than in the denatured state (39).

Structural Analysis. All of the D1D2 proteins that were crystallized belong to space group C2 (Table 2). F43V is isomorphous with the previously reported type I D1D2 crystal (15), which has cell dimensions $a = 83.7 \text{ \AA}$, $b = 30.1 \text{ \AA}$, $c = 87.5 \text{ \AA}$, and $\beta = 117.3^\circ$. The native type I D1D2 crystal changes its cell dimensions upon freezing at 110 K to $a = 82.7 \text{ \AA}$, $b = 30.4 \text{ \AA}$, $c = 88.8 \text{ \AA}$, and $\beta = 118.6^\circ$. The cell parameter change for G47S ($a = 82.2 \text{ \AA}$, $b = 29.9 \text{ \AA}$, $c = 85.5 \text{ \AA}$, and $\beta = 115.4^\circ$) relative to native D1D2 is not a sole consequence of freezing, since its cell dimensions at room temperature ($a = 81.1 \text{ \AA}$, $b = 30.8 \text{ \AA}$, $c = 86.5 \text{ \AA}$, and $\beta = 119.0^\circ$) are also different from the native type I crystal. The mutated residue Ser-47 is involved in

Table 2. Data and refinement statistics

Parameter	Native	F43V	G47S
Resolution, \AA	10–2.5	10–2.7	10–2.0
Reflections	4528	4388	10876
Completeness, %	73.1	84.9	91.0
R_{merge} , %	5.2	8.1	4.2
Model	1-178	1-178	1-178
Protein/solvent atoms	1383/90	1379/48	1385/207
Bond length, \AA	0.012	0.011	0.017
Bond angle, $^\circ$	2.2	1.9	2.1
R_{cryst} , %	18.9	15.2	20.2

the packing of G47S crystals, explaining the observed non-isomorphism for this mutant. Refinement results are shown in Table 2.

A55F failed to be crystallized in many crystallization attempts, although the sample of A55F is as pure as the other D1D2 proteins. This suggests that there may be some structural alteration of A55F that makes it difficult to crystallize.

Four native D1D2 structures are available for comparison with the mutant D1D2 structures: Protein Data Bank entries 1cdh (type I crystal; refs. 15 and 17), 1cdi (type II crystal; ref. 17), 3cd4 (16), and the type I crystal structure at 110 K. To show the degree of variability in native D1D2, we calculated the rms C_α distance at each residue ($\sum_{i=1,4} \sum_{j=1,4}^{\neq i} \Delta d_{i,j}^2/n$) among these four superimposed native D1D2 structures (Fig. 4a). This scatter of C_α positions should, to a large extent, reflect the flexibility intrinsic to each residue along the polypeptide chain. We then calculated the rms C_α distance of the mutated (F43V and G47S) versus native D1D2 structures ($\sum_{i=1,4} \Delta d_{i,\text{mut}}^2/n$). Visual inspection (Fig. 4a) showed that the rms changes in C_α positions in the mutant structures follow their natural scattering within the native structures. This suggested that the point mutations at residues 43 and 47 did not perturb the main chain conformation of D1D2.

The above analysis suggested that the altered gp120 binding properties of F43V and G47S are due entirely to their side chains. The overall structure of F43V (Fig. 4b) is especially similar to that of type I D1D2 (15, 17) with 0.09 \AA rms deviations in C_α positions, where the rms C_β distance between the two structures is 0.3 \AA . The side chains of both Phe-43 and Val-43 protrude outward essentially perpendicular to the surface of the molecules and pack against the same part of a neighboring molecule in their respective isomorphous lattices, with the latter mediated by a solvent molecule that fills the space left open by the mutation. The preservation of main chain conformation in G47S is consistent with Gly-47 being in a permissive ϕ - ψ conformation (-82° , 180° for type I crystal) and having exposed main chains in the native D1D2 structure. This allows the addition of side chains without perturbing the local conformation, although this addition does create non-isomorphism due to its involvement in crystal packing. The O^γ atom of Ser-47 is within hydrogen-bonding distance of the main chain carbonyl oxygen atom of residue 35. This interaction is not critical for binding interference, however, since G47A gives a reduction in gp120 binding affinity similar to that by G47S, as measured by competitive binding analysis (unpublished results). Therefore, G47S interferes with gp120 binding entirely due to the extra bulk in the serine side chain.

DISCUSSION

The association of gp120 with the cell surface receptor CD4 initiates the cellular entry of HIV. Using a combination of kinetics, thermodynamics, and structural analysis, we examined three mutants of CD4, expressed as soluble D1D2 proteins, that differed in their binding to gp120. Although complex overall, the early phase binding kinetics confirmed a previously less rigorous assessment of their affinity (refs. 19–22; unpublished results). To a first approximation, the F43V, A55F, and G47S mutations reduced overall affinity by 200-, 50-, and 5-fold, respectively, primarily due to a reduced association rate in each case. Phe-43 is at the center of the putative gp120 binding site, Gly-47 is at the periphery, and Ala-55 is buried beneath this gp120 binding surface (Fig. 4c). The structural integrity of F43V and G47S proteins was established by crystallography and, for F43V, by its similarity in denaturation profile to that of wild-type D1D2. A55F, however, showed an altered stability profile (see *Results*) and failed to crystallize, suggesting structural perturbation from alteration of this buried side chain. We conclude that the mutations at F43V and G47S reduce gp120 binding through a



FIG. 4. (a) The rms C_{α} distance ($\sum_{i=1,4}^{i \neq j} \Delta d_{i,j}^2/n$) at each residue of D1D2 among superimposed native structures and between native and mutant F43V or G47S structures ($\sum_{i=1,4} \Delta d_{i,mut}^2/n$). The four native D1D2 structures used for superposition are: the type I D1D2 (15, 17), type II D1D2 (17), 3CD4 (16), and the native D1D2 structure

direct effect on side chain contacts, whereas A55F does so indirectly through conformational alteration.

Our BIAcore data deviate from a simple model of bimolecular interaction. Although artifacts of BIAcore measurements can contribute to this nonlinearity, many of them have been ruled out. On the other hand, this nonlinearity may suggest multiple steps in CD4–gp120 interaction and here for simplicity and comparative purpose, we limited our analysis to the initial fast step. Moebius *et al.* (20) reported earlier that their kinetic measurements based on the interaction of CD4⁺ cells with soluble gp120 suggested, in contrast to our results, significant changes in dissociation rates for CD4 mutations. Since their measurements were done on a longer time scale (minutes to hours) and higher temperature (37°C), it is very likely that they reflected mostly a slower step in the overall CD4 and gp120 interaction. Similarly, kinetic measurements by Davis *et al.* (40) for radiolabeled sCD4 binding to bead-immobilized gp120 gave rate constants much slower than those found here. Recently, Fischer *et al.* (41) reported their BIAcore analysis of CD4–gp120 interaction where they also observed complex binding kinetics, which they fitted with a two receptor model. This gave an early phase on rate similar to our result and two off-rates that bracket our result, based on a similar time span.

The apparent affinities of these CD4 mutants to gp120, based on the early phase kinetics, are reduced mostly by changes in association rates, which are down from 3- to 50-fold, whereas dissociation rates decrease only from 1.5- to 4-fold. This result differs from several other systems in which mutations mostly affect dissociation rates (42, 43), a scenario consistent with a diffusion-limited macromolecular interaction where association rates change minimally and dissociation rates change with the stability of the complexes. In contrast, the association rate between CD4 and gp120 ($k_{on} = 8.3 \times 10^4 \text{ M}^{-1}\text{s}^{-1}$) is not diffusion-controlled. One possible basis for this limitation is a prerequisite conformational change. Structural studies of lysozyme–antibody complexes have shown that a reduction in association rates correlates with conformational adaptation on binding (44). In analogy, our situation may reflect that the initial association of CD4 and gp120 requires such conformational adaptation and that the transition state is differently affected for the different mutant variants and is high enough to allow the binding activation energy to be the rate-limiting step in association. It is likely that these CD4 mutations raise energy levels for both the transition state and the complexed state, thereby slowing association rates but leaving dissociation rates fairly unchanged. An alternative possible explanation for the effect of mutations on the association state might be differential solvation or desolvation. It is known that solvent structure can exert a significant effect in macromolecular interactions (45). Solvent structure associated with the unusually exposed phenyl group of Phe-43 could be quite different from that with its valyl counterpart, and its rate of reorganization on binding to gp120 could then also be different. In any case, a thorough understanding of the kinetics and the mechanisms of CD4 and gp120 interaction must wait for atomic details of the interaction as well as further biochemical and biophysical analysis.

We thank Dr. Craig Ogata for maintaining the Howard Hughes Medical Institute beamline X4A at NSLS, Hans-Erik Aronson for help

at 110 K determined here. The colors indicate the following: black, D1D2–D1D2; blue, F43V–D1D2; and red, G47S–D1D2. (b) Simulated annealing omit map of F43V at the region of mutation calculated with reflections between 15 and 2.7 Å spacings. Residues 42–44 were omitted in the annealing procedure ($T = 3000 \text{ K}$) and harmonic restraints are applied to the neighboring residues. Models of both type I D1D2 (magenta) and F43V (yellow) are shown. Green balls mark the C_{α} positions. (c) C_{α} spline ribbon diagram of D1D2 with side chains of Phe-43, Ala-55, and Arg-59. Residue Gly-47 is also marked.

in the data collection at X4A, Joseph Lidestri for maintaining the x-ray facility at Columbia University, Keith Deen for the G47S mutation, Margery Chaikin for preparing of D1D2 mutant expression plasmids and production cell lines, and Alem Truneh for helpful discussions. This work was supported in part by an Aaron Diamond Postdoctoral Fellowship to H.W.

1. Robey, E. & Axel, R. (1990) *Cell* **60**, 697–700.
2. Dianzani, U., Shaw, A., al-Ramadi, B. K., Kubo, R. T. & Janeway, C. A. (1992) *J. Immunol.* **148**, 678–688.
3. Janeway, C. A. (1992) *Annu. Rev. Immunol.* **10**, 645–674.
4. Vignali, D. A. & Strominger, J. L. (1994) *J. Exp. Med.* **179**, 1945–1956.
5. Turner, J. M., Brodsky, M. H., Irving, B. A., Levin, S. D., Perlmutter, R. M. & Littman, D. R. (1990) *Cell* **60**, 755–765.
6. Veillette, A., Bookman, M. A., Horak, E. M., Samelson, L. E. & Bolen, J. B. (1989) *Nature (London)* **338**, 257–259.
7. Maddon, P. J., Dalglish, A. G., McDougal, J. S., Clapham, P. R., Weiss, R. A. & Axel, R. (1986) *Cell* **47**, 333–348.
8. McDougal, J. S., Kennedy, M. S., Sligh, J. M., Cort, S. P., Mawle, A. & Nicholson, J. K. (1986) *Science* **231**, 382–385.
9. Lasky, L. A., Nakamura, G., Smith, D. H., Fennie, C., Shimasaki, C., Patzer, E., Berman, P., Gregory, T. & Capon, D. J. (1987) *Cell* **50**, 975–985.
10. Wyatt, R., Moore, J., Accola, M., Desjardin, E., Robinson, J. & Sodroski, J. (1995) *J. Virol.* **69**, 5723–5733.
11. Lifson, J. D., Feinberg, M. B., Reyes, G. R., Rabin, L., Banapour, B., Chakrabarti, S., Moss, B., Wong-Staal, F., Steimer, K. S. & Engleman, E. G. (1986) *Nature (London)* **323**, 725–728.
12. Sodroski, J., Goh, W. C., Rosen, C., Campbell, K. & Haseltine, W. A. (1986) *Nature (London)* **322**, 470–474.
13. Ho, D. D., Neumann, A. U., Perelson, A. S., Chen, W., Leonard, J. M. & Markowitz, M. (1995) *Nature (London)* **373**, 123–126.
14. Wei, X., Ghosh, S. K., Taylor, M. E., Johnson, V. A., Emini, E. A., Deutsch, P., Lifson, J. D., Bonhoeffer, S., Nowak, M. A., Hahn, B. H., Saag, M. S. & Shaw, G. M. (1995) *Nature (London)* **373**, 117–122.
15. Ryu, S.-E., Kwong, P. D., Truneh, A., Porter, T. G., Arthos, J., Rosenberg, M., Dai, X., Xuong, N., Axel, R., Sweet, R. W. & Hendrickson, W. A. (1990) *Nature (London)* **348**, 419–426.
16. Wang, J., Yan, Y., Garrett, T. P. J., Liu, J., Rodgers, D. W., Garlick, R. L., Tarr, G. E., Husain, Y., Reinherz, E. L. & Harrison, S. C. (1990) *Nature (London)* **348**, 411–418.
17. Ryu, S.-E., Truneh, A., Sweet, R. W. & Hendrickson, W. A. (1994) *Structure (London)* **2**, 59–74.
18. Brady, R. L., Dodson, E. J., Dodson, G. G., Lang, G., Davis, S. J. & Williams, A. F. (1993) *Science* **260**, 979–983.
19. Arthos, J., Deen, K. C., Chaiken, M. A., Fornwald, J. A., Sathe, G., Sattentau, Q. J., Clapham, P. R., Weiss, R. A., McDougal, J. S., Pietropaola, C., Axel, R., Truneh, A., Maddon, P. J. & Sweet, R. W. (1989) *Cell* **57**, 469–481.
20. Moebius, U., Clayton, L. K., Abraham, S., Harrison, S. C. & Reinherz, E. L. (1992) *J. Exp. Med.* **176**, 507–517.
21. Peterson, A. & Seed, B. (1988) *Cell* **54**, 65–72.
22. Brodsky, M. H., Warton, M., Myers, R. M. & Littman, D. R. (1990) *J. Immunol.* **144**, 3078–3086.
23. Deen, K. C., McDougal, S., Inacker, R., Folena-Wasserman, G., Arthos, J., Rosenberg, J., Maddon, P. J., Axel, R. & Sweet, R. W. (1988) *Nature (London)* **331**, 82–84.
24. Carr, S. A., Hemling, M. E., Folena-Wasserman, G., Sweet, R. W., Anumula, K., Barr, J. R., Huddleston, M. J. & Taylor, P. (1989) *J. Biol. Chem.* **264**, 21286–21295.
25. Brighty, D. W., Rosenberg, M. Chen, I. S. & Ivey-Hoyle, M. (1991) *Proc. Natl. Acad. Sci. USA* **88**, 7802–7805.
26. Lofas, S. & Johnsson, B. (1990) *J. Chem. Soc. Chem. Commun.* **21**, 1526–1528.
27. Johnsson, B., Lofas, S., Lindquist, G., Edstrom, A., Muller Hillgren, R.-M. & Hansson, A. (1995) *J. Mol. Recognit.* **8**, 125–131.
28. Karlsson, R., Michaelsson, A. & Mattsson, L. (1991) *J. Immunol. Methods* **145**, 229–240.
29. Tendian, S. W., Myszka, D. G., Sweet, R. W., Chaiken, I. W. & Brouillette, C. G. (1995) *Biochemistry* **34**, 6464–6474.
30. MacPherson, A. (1982) *Preparation and Analysis of Protein Crystals* (Wiley, New York).
31. Otwinowski, Z. (1990) DENZO, A Data Processing Package (Yale Univ., New Haven, CT).
32. Kabsch, W. (1988) *J. Appl. Crystallogr.* **21**, 916–924.
33. Science and Engineering Research Council (U.K.) Collaborative Computing Project 4 (1979) CCP4 (Daresbury Laboratory, Daresbury, U.K.)
34. Brunger, A. T. (1989) X-PLOR Manual (Yale Univ., New Haven, CT).
35. Jones, T. A. (1978) *J. Appl. Crystallogr.* **11**, 268–272.
36. Morton, T. A., Myszka, D. G. & Chaiken, I. M. (1995) *Anal. Biochem.* **227**, 176–185.
37. Malmqvist, M. & Granzow, R. (1994) *Methods Enzymol.* **6**, 95–98.
38. Shortle, D. & Meeker, A. (1986) *Proteins Struct. Funct. Genet.* **1**, 81–89.
39. Pakula, A. A. & Sauer, R. T. (1990) *Nature (London)* **344**, 363–364.
40. Davis, S. J., Schockmel, G. A., Somoza, C., Buck, D. W., Healey, D. G., Rieber, E. P., Reiber, C. & Williams, A. F. (1992) *Nature (London)* **358**, 76–79.
41. Fischer, P. B., Collin, M., Karlsson, G. B., James, W., Butters, T. D., Davis, S. J., Gordon, S., Dwek, R. A. & Platt, F. M. (1995) *J. Virol.* **69**, 5791–5797.
42. Larvor, M.-P., Djavadi-Ohanian, L., Friguet, B., Baleux, F. & Goldberg, M. E. (1991) *Mol. Immunol.* **28**, 523–531.
43. Cunningham, B. C. & Wells, J. A. (1993) *J. Mol. Biol.* **234**, 554–563.
44. Bhat, T. N., Bentley, G. A., Boulot, G., Greene, M. I., Tello, D., Dall'Acqua, W., Souchon, H., Schwarz, F. P., Mariuzza, R. A. & Poljak, R. J. (1994) *Proc. Natl. Acad. Sci. USA* **91**, 1089–1093.
45. Tello, D., Eisenstein, E., Schwarz, F. P., Goldbaum, F. A., Fields, B. A., Mariuzza, R. A. & Poljak, R. J. (1994) *J. Mol. Recognit.* **7**, 57–62.